Temperature Dependence of the Surface-Plasmon-induced Goos-Hanchen Shifts

C. W. Chen[1 *], H.-P. Chiang [1,2,3 #], D. P. Tsai[3,4], and P. T. Leung[1,4,5 †]

[1]Institute of Optoelectronic Sciences, National Taiwan Ocean University, Keelung, Taiwan 202, R. O. C.
[2] Institute of Physics, Academia Sinica, Taipei, Taiwan 11529, R. O. C.
[3] Instrument Technology Research Center, National Applied Research Laboratories, Hsinchu, Taiwan 300, R. O. C.
[4]Department of Physics, National Taiwan University, Taiwan 10617, R. O. C.
[5]Department of Physics, Portland State University, P. O. Box 751, Oregon 97207-0751, U. S. A.

Abstract

Optical sensing of temperature variations is explored by studying the Goos-Hanchen (GH) lateral shift of a reflected light beam from various device based on the surface plasmon (SP) excitation at metal-dielectric interfaces. Both the Kretchman and the Sarid geometry will be considered, where the temperature variations of the GH shifts associated with excitation of both the regular and the long range SP will be studied. It is found that while the SP-induced shifts and their temperature sensitivities are much greater than those from a bare metallic surface, these sensitivities are comparable between the shifts induced by the different kinds of SP, although the long range SP can in general induce much greater values in the GH shifts as reported recently in the literature.

† Corresponding author at D95880001@ntou.edu.tw
#Corresponding author at hpchiang@ntou.edu.tw
* Corresponding author at hopl@pdx.edu

Introduction

The Goos-Hanchen (GH) effect refers to the lateral shift of a well-collimated incident beam upon reflection from an interface [1,2]. Since the first observation of the effect from the shift of totally-reflected light beam at a dielectric-air interface more than sixty years ago [1], many interesting effects relating to this phenomenon have been discovered. Depending on different kinds of polarized light and material interfaces, a very rich of literature has been established covering both positive (forward) shifts and negative (backward) shifts at interfaces of a large variety of materials including insulating and conducting (metallic); isotropic and anisotropic; and natural as well as meta-materials [3-14]. For example, nontrivial GH shifts have since been studied at partially-reflecting surfaces [3] including weakly-absorbing [4-5] and metallic surfaces [6,7]; nonlinear Kerr material interfaces [8]; phase-conjugate surfaces [9]; anisotropic interfaces of antiferromagnet [10] and graphene [11]; photonic crystals [12], left-handed materials [13]; as well as other heterogeneous materials [14] .

Applications of these GH shifts have been explored from time to time for the last several decades: from designing new sensing technologies [15] to slowing down light by the negative shifts [16]. However, the generally small magnitudes in these shifts have limited such applications mostly to the laboratories; and this has motivated many researchers in recent years to explore new optical structures which will lead to significantly large GH shifts (both positive and negative shifts). One of these approaches is to exploit resonance conditions in specially-designed optical structures. Over the last two decades, for example, such large shifts have been observed from various systems including resonant absorption from gas vapor layer deposited at a transparent interface

[17], waveguides [18-20], and surface plasmon resonance (SPR) devices [21, 22].

In the SPR devices [22], attenuated total reflection (ATR) in the Kretschmann geometry was applied and a one-dimensional position-sensitive detector (PSD) was used to measure the GH shifts of the reflected beam from the prism. It was found that besides the conventional positive shift (~ wavelength λ) associated with the total reflection at the critical angle; much greater positive/negative shifts (~ 100λ) can occur along with the excitation of the SPR at the resonance angle which is slightly greater than the critical angle. Furthermore, it was reported that the sign of these shifts depends crucially on the metal film thickness which, when goes beyond a certain critical value, will make the GH shift change from positive to negative displacements. More recently, the study of these lateral shifts has been extended to the Sarid geometry [23] from which much greater GH shifts (~ 1000λ, both positive and negative) can be obtained due to the excitation of the long range surface plasmons (LRSP) [24, 25].

It is the purpose of our present work to explore the possibility of optical sensing of temperature variation by monitoring these SP-induced GH shifts. We shall focus on the Sarid geometry shown in Fig. 1 which includes the Kretschman geometry in the limit of zero thickness for the spacer layer (dielectric medium 2). Note that although the coupling across the metal film (medium 3) to excite the LRSP is strongest for a symmetric $\left(n_2 \approx n_4\right)$ geometry, it is also possible for an asymmetric $\left(n_2 \neq n_4\right)$ geometry [26]. Due to the extremely sharp resonance in the ATR reflectivity spectrum associated with the LRSP excitation, it has been exploited in the literature to achieve ultra-high sensitivity in various sensor applications [27, 28] by monitoring the change in reflectivity and phase across the very sharp resonance reflectance dip. Here we provide in the following an

alternative scheme for temperature sensing by monitoring the GH shifts associated with the SP and LRSP excitations, by demonstrating the strong temperature dependence of these shifts via numerical simulations, and by comparing them with those observed previously from a bare metallic surface which was then applied to temperature sensing with modest sensitivity [15]. We shall also see that the high temperature sensitivities for both the SP and LRSP induced shifts are of comparable magnitudes in general.

Theoretical Model

For the conventional Kretschmann geometry, it has been well-established that the SPR reflectivity can be approximated by a Lorentzian provided that (i) the loss in the metal film is relatively small, and (ii) the film thickness is much less than the wavelength of the incident light. This is accomplished via the introduction of two damping constants for the ATR geometry, namely, the radiative damping constant $\left(\text{Im}\,\Delta k^{rad}\right)$ and the internal damping constant $\left(\text{Im}\ k_x^0\text{, internal within the metal film}\right)$ [29]. While the former damping constant results from the coupling of SP to the reflected light via the presence of the prism, and the latter results from dissipation loss in the metal film; both contribute to the "width" of the SPR reflectivity curve.

It turns out that the above description is very general and can be extended to a multilayer device such as a prism-coupled waveguide system [18] and a four-layer Sarid geometry [24, 25]. We give a brief summary of the results as follows. Thus for a P- or S-polarized incident light from the prism side (see Fig. 1), the Fresnel reflection coefficients can be obtained as:

$$r_{1234} = \frac{r_{12} + r_{234}\exp(2ik_{2z}d_2)}{1 + r_{12}r_{234}\exp(2ik_{2z}d_2)}, \qquad (1)$$

with $$r_{234} = \frac{r_{23} + r_{34}\exp(2ik_{3z}d_3)}{1 + r_{23}r_{34}\exp(2ik_{3z}d_3)}, \quad (2)$$

and

$$r_{ij} = \begin{cases} \dfrac{k_{iz}/\varepsilon_i - k_{jz}/\varepsilon_j}{k_{iz}/\varepsilon_i + k_{jz}/\varepsilon_j}, & P-\text{wave} \\ \dfrac{k_{iz} - k_{jz}}{k_{iz} + k_{jz}}, & S-wave \end{cases}, \quad (3)$$

where r_{ij} are the interface reflectance (i, j =1,2,3,4); ε_i are the dielectric constants and k_{iz} are the normal components of the wave vector in each of the layers; d_2 and d_3 are the thickness of dielectric layer and metal film, respectively.

Since k_{2z} is purely imaginary under the ATR condition, hence for a separating layer of large enough thickness $(i.e.\ d_2 >> \lambda)$, we have $exp(2ik_{2z}d_2) << 1$. Under this condition, it can be shown that the reflectivity in Eq. (1) can be approximately described by two damping rates in the following form [18]:

$$r_{1234} = r_{12}\frac{k_x - [\mathrm{Re}(k_x^0) + \mathrm{Re}(\Delta k_x^{rad})] - i[Im(k_x^0) - \mathrm{Im}(\Delta k_x^{rad})]}{k_x - [\mathrm{Re}(k_x^0) + \mathrm{Re}(\Delta k_x^{rad})] - i[Im(k_x^0) + \mathrm{Im}(\Delta k_x^{rad})]}, \quad (4)$$

where the *internal damping rate* is given by:

$$\mathrm{Im}(k_x^0) \cong c_1 n_{3i}/d_3; \quad (5)$$

and the *radiation damping rate* is given by:

$$\mathrm{Im}(\Delta k_x^{rad}) = c_2\exp(ik_{2z}d_2)/d_3; \quad (6)$$

with c_1, c_2 being constants which have been studied in details in a recent work [25]; n_{3i} the imaginary part of the refractive index of the metal film; and k_x^0 in Eqs. (4) and (5) is the resonant propagation constant of the three layer system when the thickness of the

dielectric (layer 2) is taken as semi-infinite (i.e. in the absence of the prism). Note that the rate in (5) essentially accounts for the loss of plasmonic energy via absorption of the system (mainly in the metal film); and that in (6) accounts for the loss due to radiation away from the system as coupled back by the presence of the prism (since Δk_x^{rad} is essentially the difference between the two resonant wave number: with and without the presence of the prism). Hence under these approximations, the SP reflectance curve of the 4-layer system can be described by a Lorentian function of the form [18]:

$$R = \left|r_{1234}\right|^2 = \left|r_{12}\right|^2 \left(1 - \frac{4Im(k_x^0)\,\mathrm{Im}(\Delta k_x^{rad})}{\left\{k_x - [\mathrm{Re}(k_x^0) + \mathrm{Re}(\Delta k_x^{rad})]\right\}^2 + [Im(k_x^0) + \mathrm{Im}(\Delta k_x^{rad})]^2} \right) \quad . \quad (7)$$

In the following, we shall use the exact Fresnel result in Eq. (1) to calculate numerically the GH shifts associated with the SP $(d_2 = 0)$ and LRSP $(d_2 \neq 0)$, respectively; and then use the rates defined in(5) and (6) to understand the various behaviors of the numerical calculations. In order to calculate the GH shifts (D), we adopt the simple approach of the Artmann formula [30] in the form:

$$D = -\frac{1}{k}\frac{d\phi}{d\theta}, \quad (8)$$

where k is the incident wave number and θ the incident angle, respectively, while ϕ is the phase difference between the reflected and incident waves and is defined as follows:

$$\phi = \begin{cases} \arctan(\mathrm{Im}\, r / \mathrm{Re}\, r), \mathrm{Re}\, r > 0 \\ \arctan(\mathrm{Im}\, r / \mathrm{Re}\, r) + \pi, \mathrm{Re}\, r < 0, \mathrm{Im}\, r > 0 \\ \arctan(\mathrm{Im}\, r / \mathrm{Re}\, r) - \pi, \mathrm{Re}\, r < 0, \mathrm{Im}\, r > 0 \end{cases} \quad (9)$$

where $r = r_{1234}$ is the Fresnel reflection coefficient. Note that it has been shown [18] that when the resonance condition is satisfied in (7), i.e.

$$k_x = \mathrm{Re}(k_x^0) + \mathrm{Re}(\Delta k_x^{rad}), \quad (10)$$

the GH shift calculated from (8) can be approximated in the following form [18, 25]:

$$D = -\frac{2\,\mathrm{Im}(\Delta k_x^{rad})}{\mathrm{Im}(k_x^0)^2 - \mathrm{Im}(\Delta k_x^{rad})^2}\cos\theta \quad . \tag{11}$$

The temperature dependence of D arises mainly from the change in optical properties of the metal (Ag) film as the sensor temperature (T) increases. Here we briefly re-capitulate a previous model we established to describe these changes [28, 31, 32]. To begin, we model the dielectric response of the Ag film using the Drude model:

$$\hat{\varepsilon}_3 = 1 - \frac{\omega_P^2}{\omega\left(\omega + i\omega_c\right)}, \tag{12}$$

where ω_C is the collision frequency and ω_P the plasma frequency given by :

$$\omega_p = \sqrt{\frac{4\pi N e^2}{m^*}}\ , \tag{13}$$

with N and m* the density and effective mass of the electrons, respectively. Hence, assuming the variation of m* with T can be ignored [31], ω_p depends on T via volumetric effects as follows:

$$\omega_p = \omega_{p0}\,[1+\gamma(T-T_0)]^{-1/2}, \tag{14}$$

where γ is the expansion coefficient of the metal, and T_0 is a reference temperature taken to be the room temperature. The collision frequency will have contributions from both phonon-electron and electron-electron scattering:

$$\omega_c = \omega_{cp} + \omega_{ce}\ , \tag{15}$$

and can be modeled using the various scattering models in the literature. We thus obtain [32]:

$$\omega_{cp}(T) = \omega_0\,\left[\frac{2}{5} + 4\left(\frac{T}{\theta}\right)^5 \int_0^{\theta/T} \frac{z^4\,dz}{e^z - 1}\right], \tag{16}$$

where θ is the Debye temperature and ω_0 is a constant to be determined from the static limit of the above expression together with the knowledge of the d.c. conductivity [32]. In addition, we have [32]:

$$\omega_{ce}(T) = \frac{1}{12}\pi^3 \frac{\Gamma\Delta}{\hbar E_F}[(k_B T)^2 + (\hbar\omega/2\pi)^2] \text{ ,} \qquad (17)$$

where Γ and Δ are defined in Ref [31]. Thus Eqs. (12) – (17) provide a model for the temperature dependence of $\hat{n}_3 = \sqrt{\hat{\varepsilon}_3}$, which when used in Eq.(11) will lead to temperature dependent GH shifts associated with the SP and LRSP excitations.

Numerical results

To demonstrate the temperature effects on the LRSP induced GH shifts, we refer to the Sarid geometry in Fig. 1 with a high-index SF10 prism (n_1 = 1.711) and a spacer layer of glass (n_2 = 1.5) with a thickness of (d_2 = 970 nm). The metal film of thickness (d_3 = 30 nm) is taken as Ag with optical properties as described in the above temperature-dependent model. The wavelength of the incident light is fixed at 670 nm. For illustration purpose, we also consider the ideal symmetric case when the index of the external medium exactly matches that of layer (i.e. $n_4 = n_2$). The GH shifts are defined as the difference between that from an incident TM wave and that from a TE wave, which is the quantity usually measured in experiments.

Fig. 2a shows the GH shifts as a function of incident angles at various ambient temperatures. It can be seen that as reported in the literature [24, 25], shifts of the order of 10^3 λ can be reached via LRSP excitation. In addition, large variation in the GH shifts takes place as the temperature varies from 100 K to 600 K, with positive shifts at lower

temperatures and negative ones at higher temperatures. This can be understood by plotting the angular spectrum of the reflectivity as shown in Fig. 2b, in which we see that as temperature increases, the dip of the reflectance curves first decreases and then increases for $T \geq 300K$. At the same time, the widths of these curves keep on increasing as temperature increases. This implies that for lower temperatures, the internal damping (ID, Eq. (5)) is small and the radiation damping (RD, Eq. (6)) dominates so that the GH shift (Eq. (11)) becomes positive. Furthermore, it becomes more positive as the RD decreases (i.e. lower reflectance dip) and ID increases (still below RD) when temperature goes up. However, above a certain temperature (~ 300 K), the ID becomes greater than RD due to the increase in both electron-phonon and electron-electron collisions (Eqs. (16), (17)), and the GH shifts turn negative. In addition, as the temperature keeps on increasing, the RD also starts to increase (i.e. higher reflectance dip) but remains below the ID. Moreover, the increase in ID with temperature (greater width for reflectance curve) becomes far more significant, leading to an overall less negative GH shifts as appeared in Fig. 2a.

In Fig. 3, we have plotted the variation of the peak shifts as a function of temperature for both the positive (Fig. 3a) and negative (Fig. 3b) shifts. It is observed that while the nonlinear increase in shifts with temperature are much greater than those at a bare metal surface [15], there is a region just above and just below the "transition temperature (~ 300 K) in which the change in shifts are greatest. For example, if we assume a linear variation, the slope of the temperature variations for positive shifts is found to be ~ 254 nm/K for the range of T from 200 K to 250 K, and that for negative shifts to be ~ 27 nm/K for T from 300 K to 350 K. Avoiding these rapidly-varying

regions, we have shown in Fig. 3 the variation of the LRSP-induced positive GH shifts for T from 100 K to 250 K; and that for negative shifts for T from 400 K to 600 K, respectively.

In Figs. 4 and 5, we have repeated similar analysis for the Kretschman geometry in which we have set $d_2 = 0$ and $d_3 = 55$ nm for the Ag film. The qualitative features of the temperature dependence for the GH shifts in this case are very similar to those in the Sarid geometry. Compared to the results in Figs. 2 and 3 for the Sarid geometry, it is seen that while the LRSP-induced shifts are on the average greater than those from the Kretschman geometry, the *rate* of change of these GH shifts with temperature are rather comparable between the two geometries. Close to the "transition regions" (not shown), we found the approximate "linear rates" of ~ 12 nm/K for the positive shifts from T = 250 K to 300 K, and ~ 402 nm/K for the negative shifts from T = 350 K to 400 K, respectively. Thus we conclude that as temperature sensors, the Kretschman geometry and the Sarid geometry should have very comparable sensitivity, although for other sensing applications, the LRSP approach has been found with appreciable greater sensitivities [27]. In any case, both device will have much greater temperature sensitivities in the GH shifts compared to that obtained by monitoring such shifts on a bare metal surface (15) which was limited to have only a rate ~ 10^{-2} nm/K [15].

Discussion and Conclusion

In this work, we have demonstrated that the GH shifts induced by the excitations of SP [22] or LRSP [24, 25] are not only much greater than those from a bare metal surface [6], but their temperature sensitivities are also much higher than that with a bare metal surface [15]. Moreover, the two geometries (Kretschman and Sarid) have

comparable temperature sensitivities although the LRSP (Sarid) induced shifts are in general of greater values. This is consistent with what was found previously [28] when these SP sensors were applied to monitor temperatures via measurements of reflectance and phase changes. Thus it seems that although the LRSP sensor can outperform the Kretschman device in other sensing applications [27], this may not be the case in terms of temperature sensing.

Another interesting issue is that concerning the possible direct correlation between the two length scales, i.e.: the GH shift and the SP range. While it seems that the LRSP-induced shifts are indeed on the average greater than the SP-induced shifts, we are not sure the two will have a definite correlation. For this purpose, we have carried out a numerical study of the case with the "extended range surface plasmon (ERSP)" achieved using the Kou-Tamir geometry [33], in the range for the SP is even greater than that of the LRSP in the Sarid geometry. However, our preliminary results show that the GH shifts attainable from this ERSP geometry does *not* turn out necessary to be greater that those from the Sarid geometry. It is hence of interest for a future study to completely clarify the ultimate relation between these two length scales, and to study further the temperature sensitivities of ERSP-induced GH shifts.

Acknowledgments

PTL wants to thank the National Center for Theoretical Sciences and the National Taiwan University – Center for Theoretical Sciences for the support provided. We also acknowledge the financial support from National Science Council, Taiwan, ROC, under Grant numbers NSC 100-2112-M-019 -003 -MY3, NSC 100-2120-M-002-008, and NSC 100-2923-M-002-007-MY3.

References

[1] F. Goos, H. Hanchen, Ann. Phys. **1**, 333 (1947); *ibid* **5**, 251 (1949)

[2] For an earlier comprehensive review, see H. Lotsch, Optik **32**, 116 (1970); *ibid* **32**, 299; **32**, 553 (1971)

[3] W. J. Wild, C. L. Giles, Phys. Rev. A **25**, 2099 (1982)

[4] O. V. Ivanov, D. I. Sementsov, Opt. Spectrosc. **89**, 737 (2000); *ibid*: **92**, 462 (2002)

[5] H. M. Lai, S. W. Chan, Opt. Lett. **27**, 680 (2002)
H. M. Lai, S. W. Chan, W. H. Wong, J. Opt. Soc. Am. A **23,** 3208 (2006)

[6] P. T. Leung, C. W. Chan, H. P. Chiang, Opt. Comm. **276**, 206 (2007)

[7] M. Merano, A. Aiello, G. W. 't Hooft, M. P. van Exter, E. R. Eliel, J. P. Woerdman, Opt. Exp. **15**, 15928 (2007)

[8] O. Emile, T. Galystyan, A. Le Floch, F. Bretenaker, Phys. Rev. Lett. **75**, 1511 (1995); H. Zhou, X. Chen, P. Hou, C. F. Li, Opt. Lett. **33**, 1249 (2008); X. Chen, R. R. Wei, M. Shen, Z. F. Zhang, C. F. Li, Appl. Phys. B **101**, 283 (2010)

[9] B. M. Jost, A. R. Al-Rashed, B. E. A. Saleh, Phys. Rev. Lett. **81**, 2233 (1998)

[10] F. Lima, T. Dumelow, J. A. P. da Costa, E. L. Albuquerque, Europhys. Lett. **83**, 17003 (2008)

[11] C. W. J. Beenakker, R. A. Sepkhanov, A. R. Akhmerov, J. Tworzydlo, Phys. Rev. Lett. **102**, 146804 (2009)

[12] J. He, J. Yi, S. He, Opt. Exp. **14**, 3024 (2006)

[13] L. G. Wang, S. Y. Zhu, Appl. Phys. Lett. **87**, 221102 (2005); J. Appl. Phys. **98**, 43522 (2005); Appl. Phys. B **98**, 459 (2005)

[14] This includes, for example, gradient-index materials [see, e.g., W. Loffler, M. P. van Exter, G. W. ‘t Hooft, E. R. Eliel, K. Hermans, D. J. Broer, J. P. Woerdman, Opt. Comm. **283**, 3367 (2010)]; as well as inhomegeneous composite materials [see, e.g., B. Zhao and L. Gao, Opt. Exp. **17**, 21433 (2009); C. W. Chen, Y. W. Gu, H. P. Chiang, E. J. Sanchez, P. T. Leung, Appl. Phys. B, in press (2011)]

[15] C. W. Chen, W. C. Lin, L. S. Liao, Z. H. Lin, H. P. Chiang, P. T. Leung, E. Sijercic, W. S. Tse, Appl. Opt. **46**, 5347 (2007)

[16] K. L. Tsakmakidis, A. D. Boardman, O. Hess, Nature **450**, 397 (2007)

[17] E. Pfleghaar, A. Marseille, A. Weis, Phys. Rev. Lett. **70**, 2281 (1993)

[18] X. Liu, Z. Cao, P. Zhu, Q. Shen, X. Liu, Phys. Rev. E **73**, 056617 (2006); T. Okamoto, I. Yamagushi, Opt. Rev. **4**, 354 (1997)

[19] X. Liu, Q. Yang, Z. Qiao, T. Li, P. Zhu, Z. Cao, Opt. Comm. **283**, 2681 (2010)

[20] J. Hao, H. Li, C. Yin, Z. Cao, J. Opt. Soc. Am. B **27**, 1305 (2010)

[21] S. L. Chuang, J. Opt. Soc. Am. A **3**, 593 (1986)

[22] X. Yin, L. Hesselink, Z. Liu, N. Fang, X. Zhang, Appl. Phys. Lett. **85**, 372 (2004); X. Yin, L. Hesselink, Appl. Phys. Lett. **89**, 261108 (2006)

[23] D. Sarid, Phys. Rev. Lett. **47**, 1927 (1981)

[24] G. Sui, L. Cheng, L. Chen, Opt. Comm. **284**, 1553 (2011)

[25] L. Chen, X. Liu, Z. Cao, S. Zhuang, J. Opt. **13**, 035002 (2011)

[26] L. Wendler, R. Haupt, J. Appl. Phys. **59**, 3289 (1986)

[27] S. A.W. Wark, H. J. Lee, R. M. Corn, Anal. Chem. **77**, 3904 (2005)

[28] C. W. Chen, C. H. Lin, H. P. Chiang, Y. C. Liu, P. T. Leung, W. S. Tse, Appl. Phys. A **89**, 377 (2007)

[29] H. Raether, *Surface Plasmons on Smooth and Rough Surfaces and on Gratings* (Springer, Berlin) (1988)

[30] K. Artmann, Ann. Phys. **2**, 87 (1948)

[31] H. P. Chiang, Y. C. Wang, P. T. Leung, and W. S. Tse, Opt. Comm. **188,** 283 (2001)

[32] Most of the details for the temperature model can be found in H. P. Chiang, P. T. Leung, W. S. Tse, Solid State Commun. **101**, 45 (1997)

[33] F. Y. Kou, T. Tamir, Opt. Lett. **12**, 367 (1987)

Figure Captions

1. Configuration of the Sarid geometry studied in our simulations.
2. Plots of the angular spectra for (a) the GH shifts and (b) the reflectance associated with the LRSP excitation in the Sarid geometry at various temperatures from 100 K to 600 K.
3. Plot of the peak GH shifts as a function of temperature for both the positive and negative shifts for the Sarid geometry away form the “transition regions”.
4. Similar to Fig. 2, but for the case of the Kretschman geometry.
5. Similar to Fig. 3, but for the case of the Kretschman geometry.

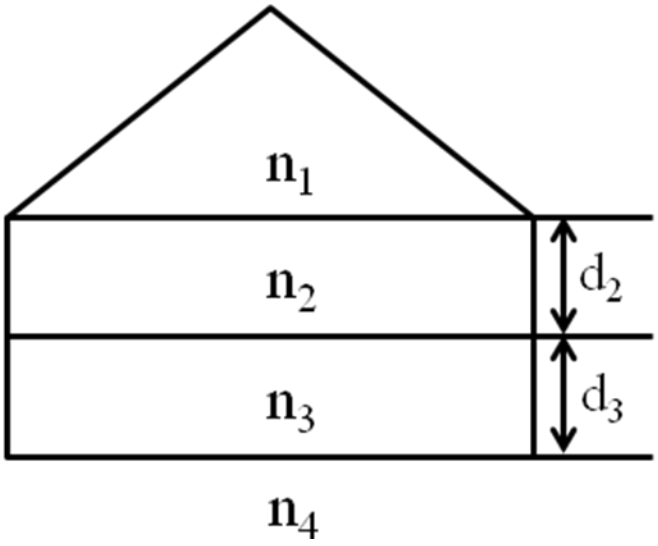

Fig. 1

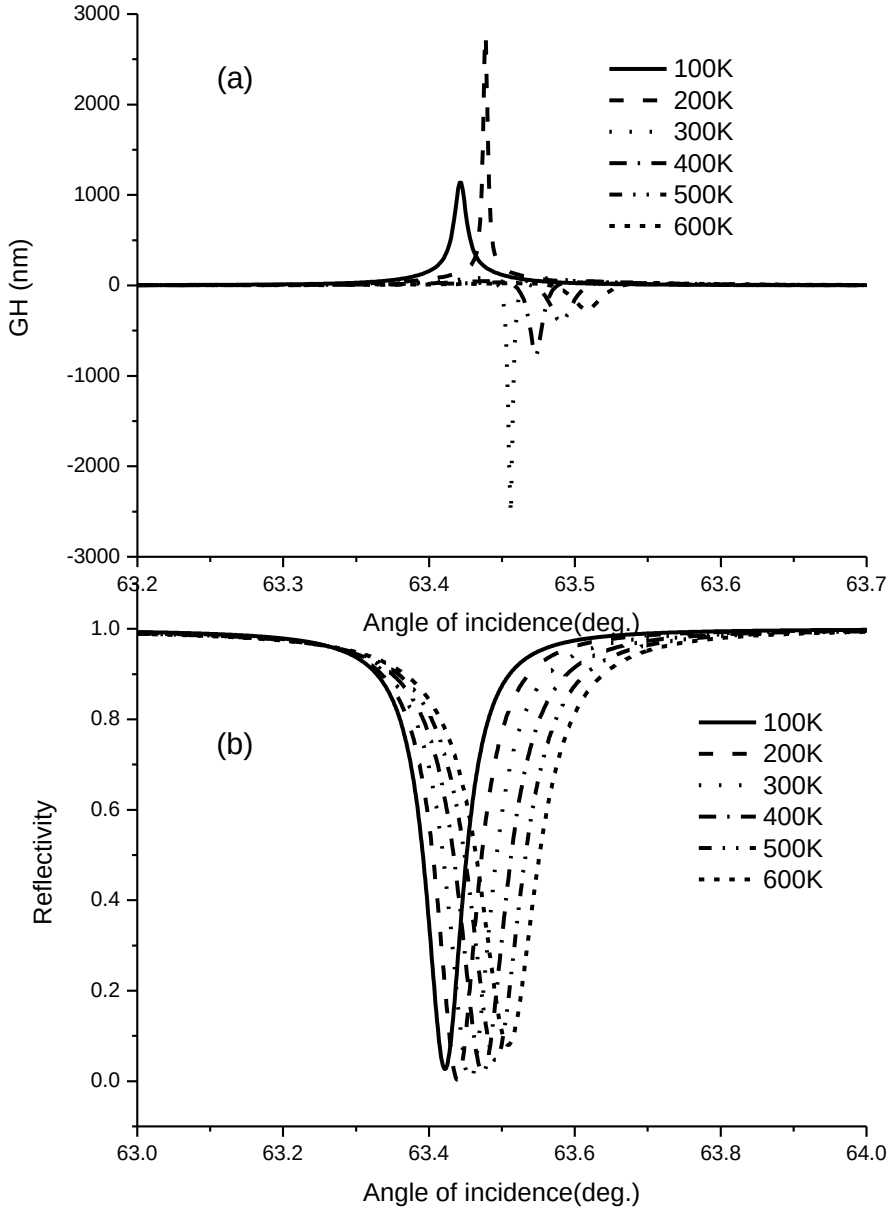
(a)
100K
200K
300K
400K
500K
600K
GH (nm)
3000
2000
1000
0
-1000
-2000
-3000
63.2
63.3
63.4
63.5
63.6
63.7
Angle of incidence(deg.)
(b)
100K
200K
300K
400K
500K
600K
Reflectivity
1.0
0.8
0.6
0.4
0.2
0.0
63.0
63.2
63.4
63.6
63.8
64.0
Angle of incidence(deg.)

Fig. 2

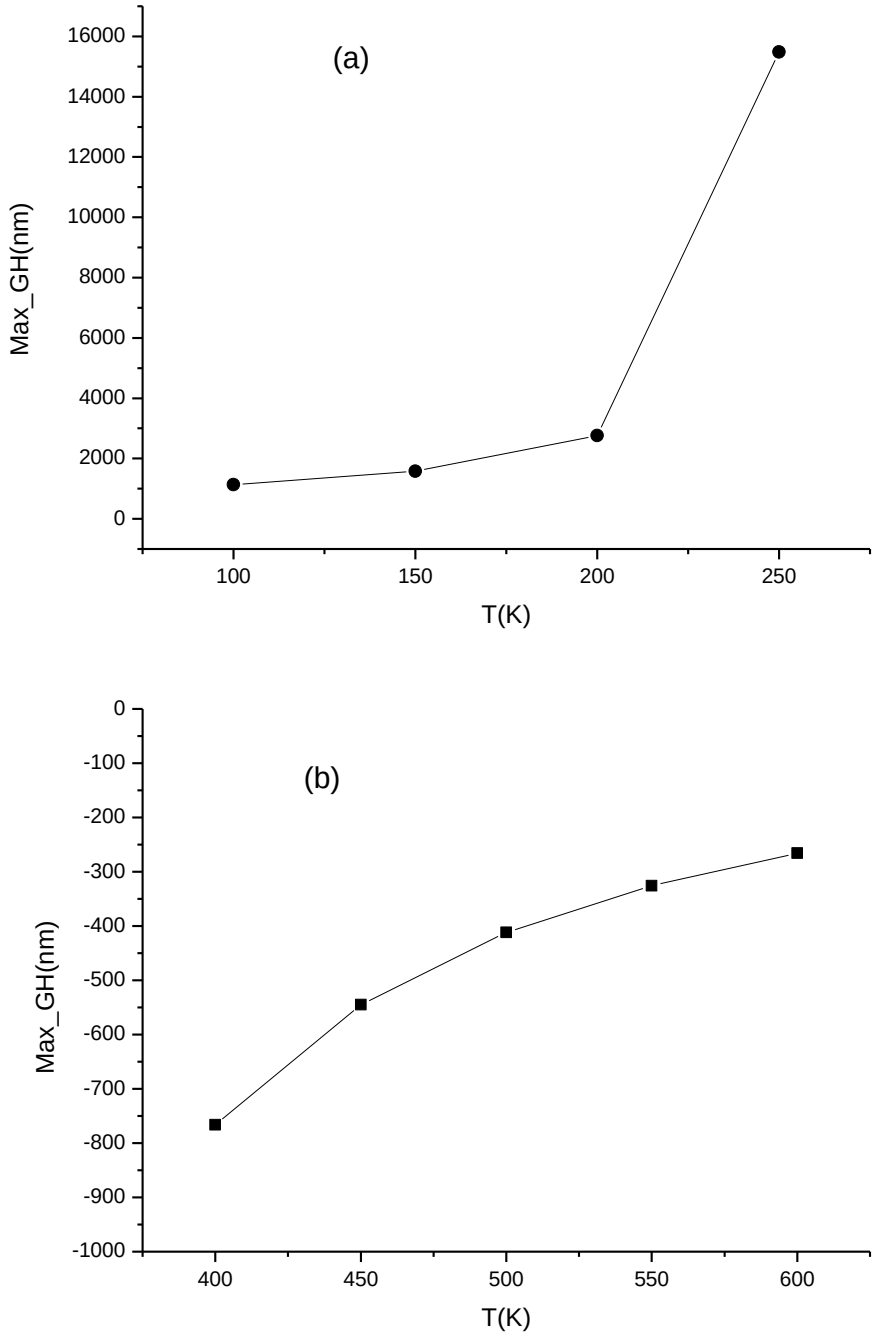
(a)
Max_GH(nm)
16000
14000
12000
10000
8000
6000
4000
2000
0
100
150
200
250
T(K)
(b)
Max_GH(nm)
0
-100
-200
-300
-400
-500
-600
-700
-800
-900
-1000
400
450
500
550
600
T(K)

Fig. 3

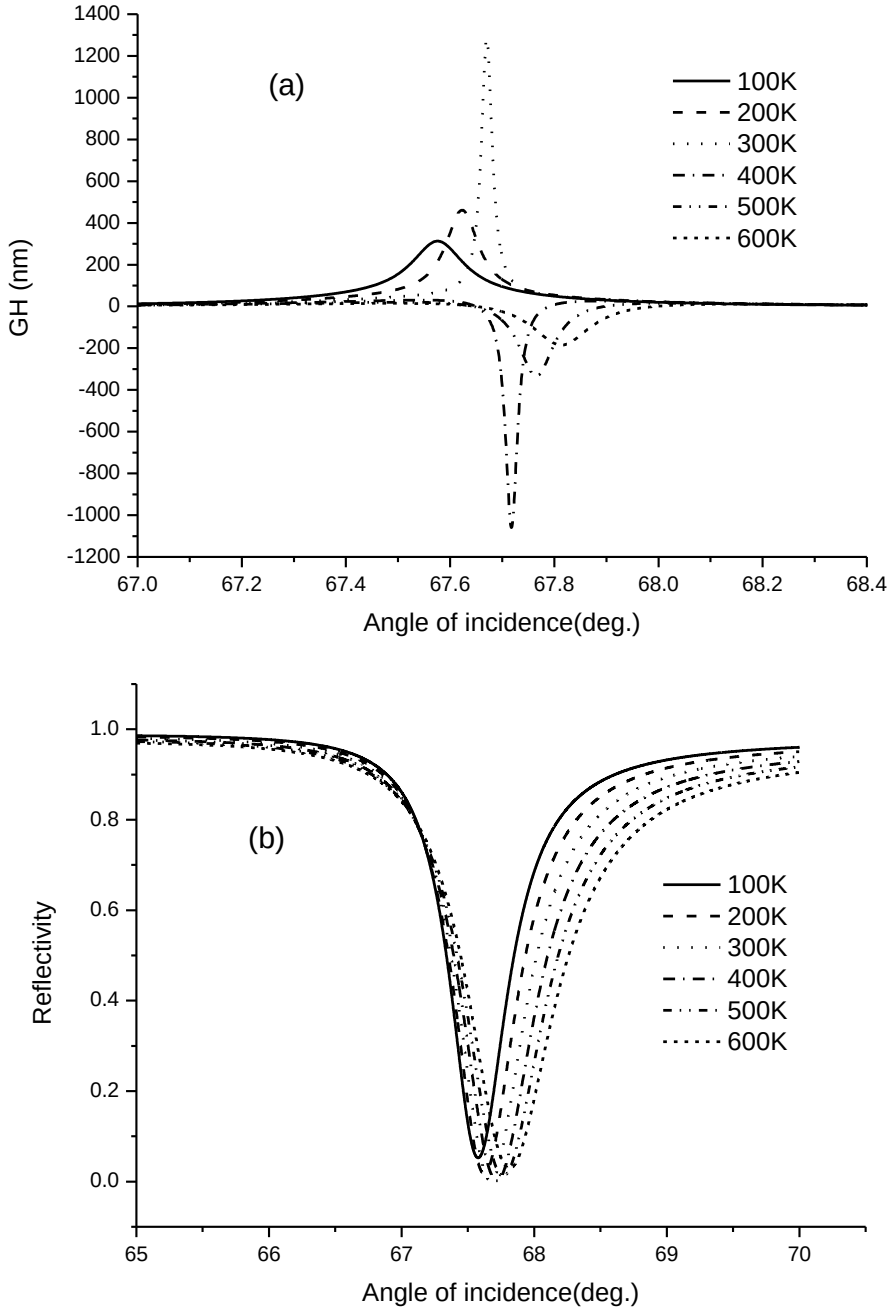
(a)
100K
200K
300K
400K
500K
600K
GH (nm)
1400
1200
1000
800
600
400
200
0
-200
-400
-600
-800
-1000
-1200
67.0
67.2
67.4
67.6
67.8
68.0
68.2
68.4
Angle of incidence(deg.)
(b)
100K
200K
300K
400K
500K
600K
Reflectivity
1.0
0.8
0.6
0.4
0.2
0.0
65
66
67
68
69
70
Angle of incidence(deg.)

Fig. 4

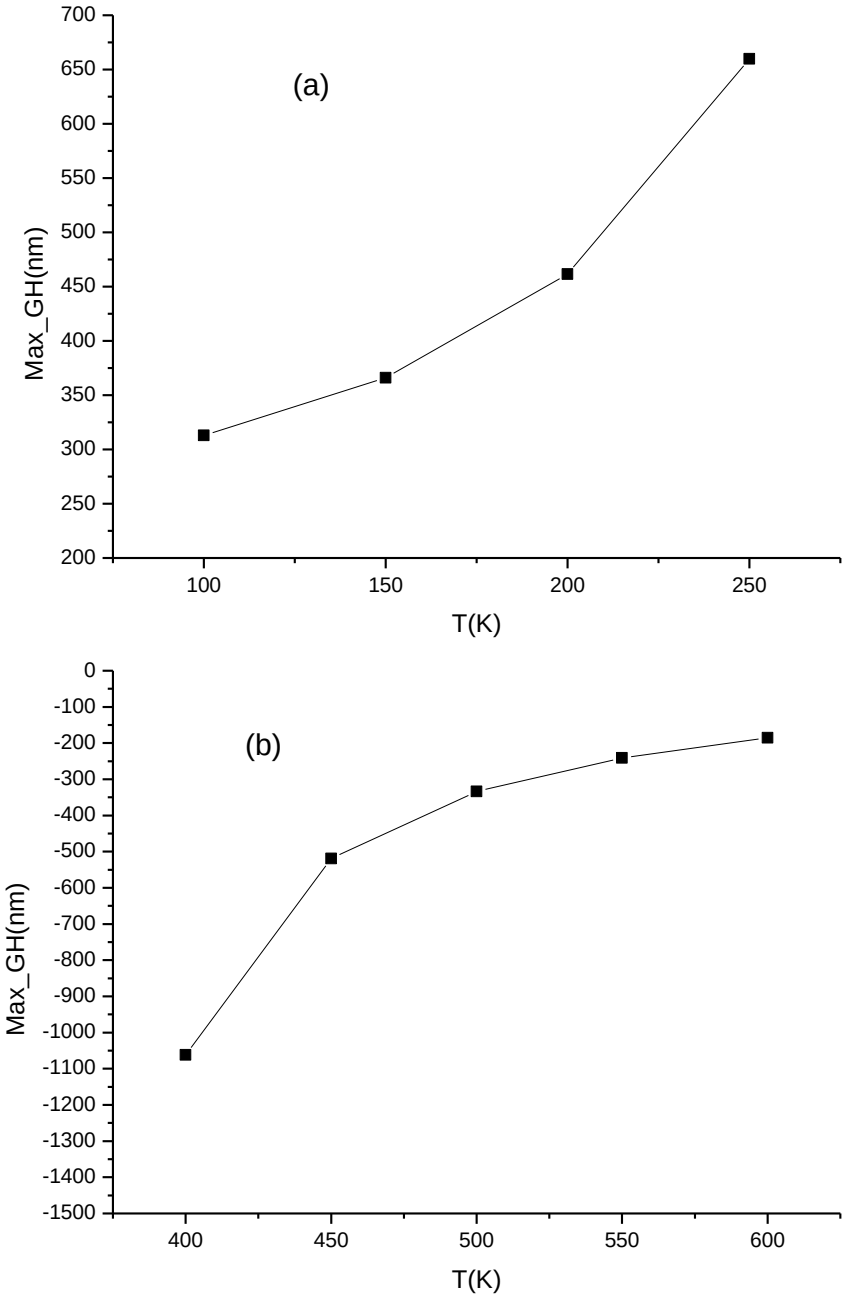
(a)
Max_GH(nm)
700
650
600
550
500
450
400
350
300
250
200
100
150
200
250
T(K)
(b)
Max_GH(nm)
0
-100
-200
-300
-400
-500
-600
-700
-800
-900
-1000
-1100
-1200
-1300
-1400
-1500
400
450
500
550
600
T(K)

Fig. 5